

# Revealing Transition in Fall-off Rates of spin- $s$ Ising Model through Multiqudit Graph states

Debkanta Ghosh, Keshav Das Agarwal, Pritam Halder, Aditi Sen(De)

Harish-Chandra Research Institute, A CI of Homi Bhabha National Institute, Chhatmag Road, Jhansi, Allahabad - 211019, India

A variable-range interacting Ising model with spin-1/2 particles exhibits distinct behavior depending on the fall-off rates in the range of interactions, notably non-local (NL), quasi-local (QL), and local. It is unknown if such a transition occurs in this model with an arbitrary spin quantum number. We establish its existence by analyzing the profiles of entanglement entropy, mutual information, and genuine multipartite entanglement (GME) of the weighted graph state (WGS), which is prepared when the multi-level maximally coherent state at each site evolves according to the spin- $s$  Ising Hamiltonian. Specifically, we demonstrate that the scaling of time-averaged mutual information and the divergence in the first derivative of GME with respect to the fall-off rate in the WGS can indicate the transition point from NL to QL, which scales logarithmically with individual spin dimension. Additionally, we suggest that the existence of a saturation value of a finite number of qudits capable of mimicking the GME pattern of an arbitrarily large system-size can reveal the second transition point between quasi-local and local regions.

## I. INTRODUCTION

The overwhelming focus of theoretical breakthroughs in quantum technologies involves mostly two-level quantum systems (qubits), although the majority of physical systems contain several levels that can only be approximated as qubit configuration [1]. Moreover, multilevel quantum systems known as qudits exhibit a non-trivial entanglement structure [2–4], which can also be confirmed by their violation of Bell inequalities [5–7]. They are also demonstrated to provide superior performance compared to their two-level counterparts in a myriad of quantum information processing tasks, including quantum secure key rates [8–16], quantum simulation and computation [17, 18], quantum telecloning [19, 20], the robust test of quantum steering [21, 22], dense coding protocol against noise [23], quantum thermal machines [24–30]. Additionally, quantum spin models like nearest-neighbor and next-nearest-neighbor Heisenberg models with spin-1 and spin 3/2, bilinear-biquadratic spin- $s$  models [31–39] may display rich phase diagrams [40–42] which cannot be found with spin-1/2 chains. Along with theoretical developments, experimental evidence shows that qudit-based quantum computers [43–55] are more efficient than qubit-based ones due to the larger computing space of each particle and improved error correction codes [56–62].

In recent years, there has been a significant surge in interest to extend the studies of many-body systems with short-range (SR) interactions to those with variable-range (VR) ones. In this VR interacting Hamiltonian, the interaction between pair of particles,  $(i, j)$ , residing at a distance  $r = |i - j|$ , falls off as  $g_{ij} \propto 1/r^\alpha$  with  $\alpha > 0$  representing the range of interactions [63–66]. Such systems are experimentally accessible in physical systems such as in trapped ions [67–73], Rydberg atoms [74, 75], ultracold atoms in optical lattices [76–80], along with superconducting qubits [81, 82]. In both equilibrium and out of equilibrium scenarios, by varying the fall-off parameter  $\alpha$ , unique observations including dynamical quantum phase transition [83–86], metastable phases [87, 88], and information scrambling [89–91] are reported, which are otherwise absent in SR interacting systems. Interestingly, it has been demonstrated that long-range (LR) interactions have

positive impact on generating highly multipartite entangled states [92, 93], quantum heat engine [94], sensing [95, 96], state transfer [97, 98] and computation [99, 100]. The change in behavior of numerous quantities such as entanglement entropy and classical correlation with fall-off rate  $\alpha$  indicating the transition from short-range to LR systems is distinct from the critical points associated with quantum phase transition when gapped to gapless transition occurs [63]. Even in spin-1/2 systems, only a few studies have been conducted to detect  $\alpha$ -transition points through the dynamical state [93, 101–106]. This work will primarily focus on the spin- $s$  Ising model, for which the presence of such transition is still unresolved.

Extracting captivating physics from systems involving dual complexity arising from multiple energy levels and LR interactions poses insurmountable analytical and numerical challenges. In this work, we provide arguments to characterize such spin- $s$  LR systems based on the strength and the range of interactions. In particular, our work has three-fold implications – (1) a proposal for creating genuine multipartite entangled higher-dimensional weighted graph state (WGS), (2) establishing the existence as well as the precise prediction of transition in fall-off rates with increasing local spin quantum number, and (3) establishing the dynamical profile of entanglement and total correlations of arbitrary dimensional WGS as a possible tool to predict transition between SR and LR interactions.

We consider the properties of dynamical weighted graph state generated by long-range interacting spin- $s$  Hamiltonian with interaction strength, which is analogous to the creation of qudit cluster state, the backbone of higher dimensional measurement-based quantum computation (MBQC) [43]. We demonstrate that the scaling of entanglement entropy changes from an area law to a volume law depending on the range of interactions and the local spin dimension. This crude prediction becomes more precise when the time-averaged mutual information (MI) between two qudits having relatively short distance exhibits distinct behavior in the quasi-local (QL) and nonlocal regimes. The divergence observed in the first derivative of the genuine multipartite entanglement (GME) measure with respect to fall-off rate further supports this prediction. Both MI and GME determine that  $\alpha$ -transition from NL to QL domain scales as  $\log_2 d$  with  $d$  being the dimension of the

local sites of the chain which matches exactly with the well studied spin-1/2 case [103].

None of these values are capable of indicating the quasi-local to local transitions inherent in the spin-1/2 transverse Ising model. However, we suggest that the system-dependence of GME, especially the threshold system-size above which the GGM pattern remains unaltered with the variation of  $\alpha$  for a fixed dimension can possibly signal the presence of QL to local transition even in the spin- $s$  Ising model.

The paper is organised in the following manner. In Sec. II, we briefly introduce the structure of higher dimensional WGS generated by spin- $s$  long-range Ising Hamiltonian and the form of reduced density matrices calculated by PEPS formalism. The possible transition of fall-off rates from NL to (quasi)local regime in spin- $s$  Ising model is predicted from the patterns of entanglement entropy in Sec. III A, mutual information in Sec. III B, and GGM in Sec. III C. We discuss saturation value of time-averaged GGM with increasing system-size in Sec. IV which signals to a probable  $\alpha$ -transition from QL to local interacting higher dimensional system (similar to spin-1/2 case) before concluding in Sec. V.

## II. GENERATION OF MULTIQUDIT WEIGHTED GRAPH STATE

An undirected finite graph  $G$  is described by the pair  $(V, E)$ , where  $V = \{1, 2, \dots, N\}$  is a finite set of vertices and  $E \subseteq [V]^2$  is the set of edges, connecting the vertices. The  $d$ -dimensional weighted graph state can be generated by initializing each vertex with a qudit in  $|+\rangle_d = \frac{1}{\sqrt{d}} \sum_{m=0}^{d-1} |m\rangle$  state and evolving the each pair of qudits,  $(i, j)$ , with the unitary  $U_{ij}(t) = e^{-ig_{ij}H_{ij}t}$ . Here  $H_{ij}$  is a two-qudit interacting Hamiltonian  $H_{ij} = \sum_{k,l=0}^{d-1} kl |kl\rangle_{ij} \langle kl|_{ij}$ , leading to the total Hamiltonian containing  $N$  sites with open boundary condition for the system given by  $H = \sum_{i,j=1}^N g_{ij}H_{ij}$ . Here  $g_{ij} = \frac{1}{r\alpha}$ , with  $|i-j| = r$  represents the variable-range interaction strength between two qudits,  $i$  and  $j$ .

Therefore, the  $N$ -qudit weighted graph state produced after time  $t$  reads as

$$\begin{aligned} |\psi(t)\rangle_N &= \prod_{i<j} U_{ij}(t) |+\rangle^{\otimes N} \\ &= \frac{1}{d^{\frac{N}{2}}} \sum_{\eta=0}^{d^N-1} \left( \prod_{\substack{i,j=1 \\ i<j}}^N \exp(ia_i a_j g_{ij} t) |\eta\rangle \right), \end{aligned} \quad (1)$$

where  $|\eta\rangle \equiv |a_1 a_2 \dots a_N\rangle$  with  $a_i \in \{0, 1, \dots, d-1\}$  represents the computational basis and can be written as  $\eta = \sum_{i=1}^N a_i d^{N-i}$ , i.e., decimal equivalent of computational basis  $|a_1 a_2 \dots a_N\rangle$ . Note that the higher-dimensional cluster state and its properties have been studied [43] where the evolving Ising Hamiltonian is nearest-neighbour. The multi-qudit weighted graph state involving variable-range interaction and its entanglement properties are not addressed before. Furthermore, such study leads to entanglement-based methods in the

framework of the cluster state to prove the existence of transition in fall-off rate of a long-range spin- $s$  Ising Hamiltonian with  $s > 1/2$  (note that dimension  $d$ , of the individual spin quantum number,  $s$  is related as  $d = 2s + 1$ ). To achieve the goal, we require to compute reduced density matrices of a subsystem, following the generalized PEPS formalism [107, 108]. For example, the single-site reduced density matrix for the first site takes the form as

$$[\rho_1]_{kl} = \frac{1}{d} \prod_{r=2}^N \left( \frac{1}{d} \sum_{p=0}^{d-1} \exp[i(k-l)p g_{1r} t] \right), \quad (2)$$

where  $g_{1r}$  denotes the interaction strength between the first site and the site  $r$ . In a similar fashion, it is possible to obtain all the reduced density matrices of the dynamical state after making arbitrary partition in the system (see Appendix. A).

## III. DETECTION OF TRANSITION FROM NON-LOCAL TO QUASI-LOCAL VIA INFORMATION-THEORETIC METHOD

By varying the range of interactions  $\alpha$ , the system-Hamiltonian can change its range of interaction from nearest-neighbour to long-range. In spin-1/2 system, it is known that transition in  $\alpha$  referred to as  $\alpha_2^*$  for the famous Ising model occurs at  $\alpha_2^* = 1$  (from nonlocal to quasi-local regimes), can be confirmed from the scaling of the correlation function in the ground state [109], the dynamical behavior of entanglement entropy of the WGS [110], dynamics of entanglement growth through half-block entropy [111] and the pattern of mutual information after the sudden quench [112].

Our goal here is to predict this transition, denoted as  $\alpha_d^*$  for arbitrary spin- $s$  Ising model. To establish it, we first focus our attention on the scaling law of block entanglement entropy although it provides a coarse-grained representation of the variation in the  $\alpha_d^*$ . We then demonstrate that the most precise estimation of  $\alpha_d^*$  can be obtained from the analysis of mutual information and multipartite entanglement measure.

### A. Transition predicted via entanglement entropy

Block entanglement entropy of a pure state  $|\psi\rangle$  divided into two parts,  $A = \{1, 2, \dots, L\}$  and  $\bar{A}$  with  $A \cup \bar{A} \equiv N$  is defined as  $E_L \equiv S(\rho_A) = -\text{Tr}(\rho_A \log_2 \rho_A)$  where  $\rho_A = \text{Tr}_{\bar{A}} |\psi\rangle \langle \psi|$  with  $|A| = L \leq N$  and  $S(\star)$  denotes the von Neumann entropy (vN). In one-dimensional spin models, when  $E_L \sim L$ , the subsystem  $A$  carries maximum vN which increases as  $|A|$  is enlarged, showing the *volume law* scaling while  $E_L \sim \log L$  indicating a *sub-volume law* and in case of *area law*,  $S(\rho_A) < \partial A = \text{constant}, \forall L$ , with  $\partial A$  being the boundary shared between  $A$  and  $\bar{A}$ .

Before going beyond the individual dimension  $d > 2$ , let us first notice that the entanglement entropy of a WGS generated with spin-1/2 Ising model saturates for  $\alpha_2^* > 1.3$  for a fixed time whereas for low values of  $\alpha$ , upto  $L = 10$ , we get the signature of volume law as  $S_L$  is seemingly increasing (see Ref.

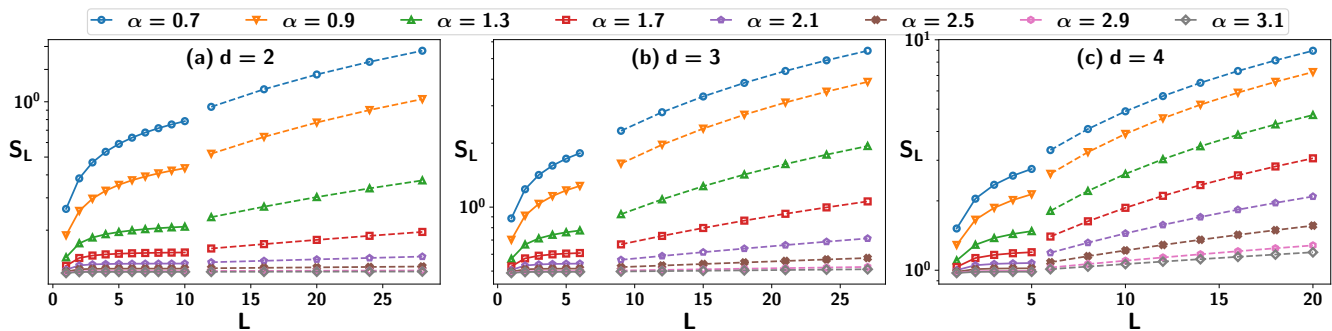


FIG. 1. (Color online.) Block entanglement entropy,  $S_L$  (vertical axis) with block length  $L$  (horizontal axis). Here system-size  $N = 10^3$  and  $t = 0.5$ . The exact values of  $S_L$  upto  $L = 10, 6, 5$  for local spin dimension  $d = 2, 3$ , and 4 are given by solid lines, whereas dashed lines represent the upper bound,  $U_L$  which possibly indicate that  $S_L$  follows the volume law. The effect of local spin dimension  $d$  can be seen since  $\alpha$  values upto which the area law can be found increases with increasing  $d$ . Note that  $U_L$  is calculated by taking  $L_j = 5, 3$ , and 2 for  $d = 2, 3$ , and 4 respectively. All the axes are dimensionless.

[110] in this respect). For higher values of  $L$ , one can note that  $S_L \leq \sum_{j=1}^{N-1} S_{L_j, L_{j+1}} - \sum_{j=2}^{N-1} S_{L_j} \equiv U_L$  where  $L_j$  denotes the sub-block of length  $L/N$ , whereas  $|L_j, L_{j+1}| = 2L/N$ .

In case of spin- $s$  Ising model used for dynamics, the behavior of  $S_L$  quantitatively remains same as in the case of spin-1/2 model although we observe that  $\alpha_d^* > \alpha_{\bar{d}}^*$  with  $d > \bar{d}$ . In particular calculating  $S_L$  with  $L = 6, 5$  [113] of  $d = 3, 4$  respectively, the area law of  $S_L$  is found when  $\alpha_3 \gtrsim 1.7$ , and  $\alpha_4 \gtrsim 2.1$  for spin-1 and spin-3/2 respectively. On the other hand, We find that the slope of  $U_L$  monotonically increases with different tangents as  $\alpha$  decreases, thereby suggesting probable entanglement volume law for small values of  $\alpha$  (see Fig. 1 for exact calculation and  $U_L$  for different values of  $\alpha$ ). Therefore, the exact nature of the entanglement entropy law cannot be concluded for low  $\alpha$  although it possibly indicates volume law in contrast to area law for high  $\alpha$  values. It strongly indicates that  $\alpha$ -transition exist even for transverse variable-range spin- $s$  Ising model with  $s > 1/2$  although precise transition point cannot be obtained through entanglement entropy.

## B. Identifying transition from trends in mutual information

The quantum mutual information,  $I(A : B) \equiv I(\rho_{AB}) = S(\rho_A) + S(\rho_B) - S(\rho_{AB})$ , quantifies the amount of total correlation, both classical and quantum, present in  $\rho_{AB}$  shared between two subsystems,  $A$  and  $B$ . In our case, we compute  $I(A : B)$  between two sites separated by distance  $r$ , i.e., we will demonstrate that for a fixed  $\alpha$ , the behavior of  $I(\alpha, r, t)$  with the variation of time for different values of  $r$  can indicate the transition point present in  $\alpha$ , thereby confirming the indication obtained from entanglement entropy. Analyzing the pattern of  $I(\alpha, r, t)$ , let us illustrate that the existence and the precise determination of  $\alpha_d^*$  is possible.

*Evidence of  $\alpha_d^* \forall d$ .* For small  $\alpha$  values and for fixed  $r$ ,  $I(\alpha, r, t)$  increases with the increase of  $t$ , reaches maximum for some  $t$  value, and then decreases before vanishing. Importantly, such feature holds for all values of  $r$  although

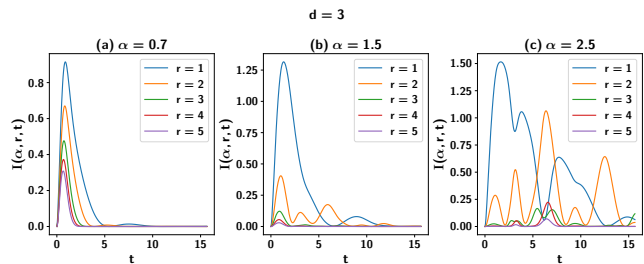


FIG. 2. (Color online.) Mutual information,  $I(\alpha, r, t)$  (vertical axis) between two distant qutrits against time  $t$  (horizontal axis) for the different values of  $\alpha = 0.7, 1.5, 2.5$  with  $N = 10^3$  for qutrits ( $d = 3$ ) in 1D lattice with open boundary condition. Different lines represent different values of distance  $r$  between two qutrits of the system. All the axes are dimensionless.

maximum of  $I(\alpha, r, t)$  monotonically decreases with  $r$ . On the other hand, with the increase of  $\alpha$ , more oscillations in  $I(\alpha, r, t)$  with time appears although substantially high values of  $I(\alpha, r, t)$  is observed between nearest-neighbor qutrits compared to the same between any two distant sites with  $r > 1$ , as depicted in Fig. 2 for  $d = 3$  (and see Fig. 9 for  $d = 2$  in Appendix B). Like entanglement entropy, the dynamics of mutual information again indicates that the transition in the fall-off rate known for spin-1/2 Ising model persists even for higher spin quantum number.

*Precise indication of  $\alpha_d^*$ .* To determine  $\alpha_d^*$ , we rely upon trends of the time-averaged mutual information  $\langle I \rangle_t = \frac{1}{t_0} \int_0^{t_0} I(\alpha, r, t) dt$  for a fixed  $\alpha$  and  $r$ . From the behavior of  $I(\alpha, r, t)$  with  $t$ , we can safely assume that  $t_0$  can be some value  $\geq 2\pi$  which is taken to be  $15\pi$  in our calculation. In case of large separation distance ( $r \gtrsim 10$ ),  $\langle I \rangle_t$  has a power law scaling, i.e.,  $\log \langle I \rangle_t \sim -\tilde{B}_\alpha \log r$ . Nonetheless, in case of small separation distance, i.e.,  $r \lesssim 10$ ,  $\log \langle I \rangle_t$  shows different scaling with  $\log r$ , i.e.,  $\log \langle I \rangle_t \sim -\tilde{A}_\alpha \log r$  (linear) for small  $\alpha$  ( $\alpha \ll 1$ ) while  $\log \langle I \rangle_t \sim -\tilde{A}_\alpha (\log r)^2$  (quadratic) with for  $\alpha \gg 1$  (see Fig. 3). Therefore, from the best fit of

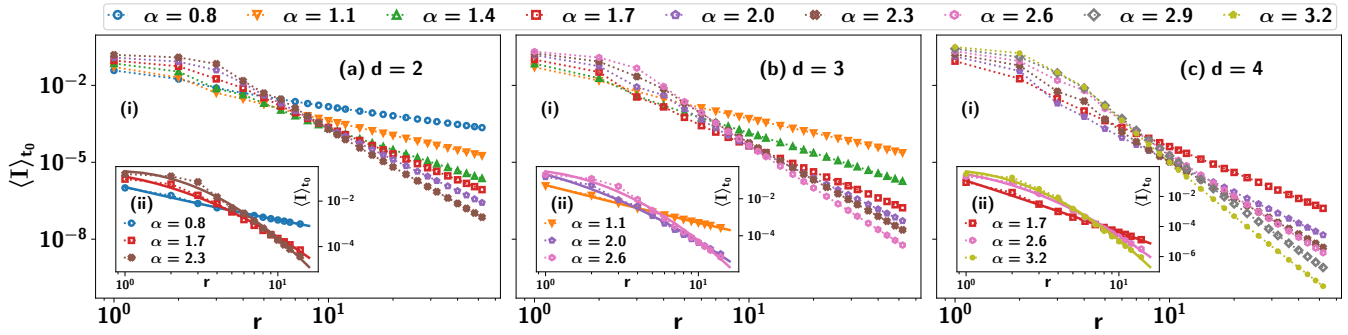


FIG. 3. (Color online.) Time-averaged of mutual information,  $(\langle I \rangle_t(\alpha, r))$ , (ordinate) against the distance between two qudits,  $r$  (abscissa) for the system-size  $N = 4000$  in logarithmic scale. The averaging is performed over the time from  $t = 0$  to  $t = 15\pi$ . While  $\log I$  decreases linearly with  $\log r$  at large  $r$  for all  $\alpha$ , its behavior changes from linear in non-local to quadratic in quasi-local domains. The quadratic fitting is done from  $r = 1$  to  $r = 15$  which shows good agreement and is shown in the insets (a),(b) and (c)(ii). All the axes are dimensionless.

the scaling  $\log \langle I \rangle_t(\alpha, r) = -\tilde{A}_\alpha (\log r)^2 - \tilde{B}_\alpha \log r + \tilde{C}_\alpha$  for  $r \lesssim 10$ ,  $\tilde{A}_\alpha$  captures the transition point,  $\alpha_d^*$  which we will show that it is indeed the case.

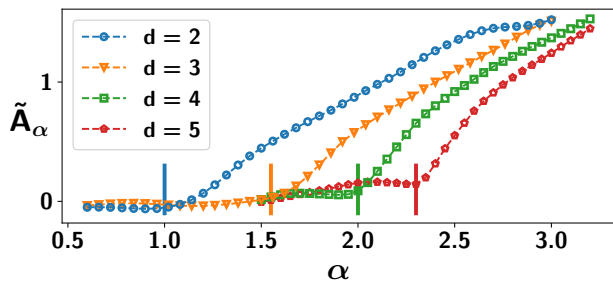


FIG. 4. (Color online.) Distinction of non-local regime from the (quasi) local one in the variable-range spin- $s$  Ising chain. The quadratic coefficients  $\tilde{A}$  (vertical axis) used in the best fit  $\log \langle I \rangle_t \sim -\tilde{A}_\alpha (\log r)^2$  against fall-off rate  $\alpha$  (horizontal axis). For small  $r$  values,  $\tilde{A} \sim 0$  in  $\alpha \lesssim 1, 1.0, 1.55, 2.0,$  and  $2.3$  for  $d = 2, 3, 4, 5$  respectively, indicating transition from NL to (quasi)local regimes of the Ising model. These transition points are marked by a vertical line for qudits. Both the axes are dimensionless.

For qubits,  $\alpha_2^* = 1$  is known to be the transition point between NL and QL regimes and we indeed observe that in the NL regime  $\langle I \rangle_t$  shows a polynomial decrease with  $r$  for short distance, having vanishing quadratic coefficient  $\tilde{A}_\alpha$  for  $\alpha \lesssim \alpha_2^* = 1$  (see Fig. 4). Further in the QL and the local regimes ( $\alpha > 1$ ), the quadratic behavior of  $\log \langle I \rangle_t$  with  $\log r$  (for small  $r$ ) leads to the linear increase of  $\tilde{A}_\alpha$  with increasing  $\alpha$  near  $\alpha_2^* = 1$ . When the lattice is built with spin- $s$  particles, the similar behavior of  $\langle I \rangle_t$  emerges for  $r \lesssim 10$ . In particular, the vanishing value of  $\tilde{A}_\alpha$  determines  $\alpha_d^*$  which is approximately 1.55 for spin-1,  $\sim 2.0$  for spin-3/2 and  $\sim 2.3$  for spin-2 lattices. These values suggest a logarithmic dependence of  $\alpha_d^*$  on the individual dimension  $d$ . Therefore, we conjecture that the NL regime increases monotonically with  $d$ , almost

logarithmically with the increasing individual spin dimension in the lattice. We establish this further via the investigations of the time averaged genuine multipartite entanglement content of the multi-qudit WGS. Since spin- $s$  transverse Ising lattice with long-range interactions is not easy to handle, both analytically and numerically, the analysis carried out here also suggests a potential information-theoretic method based on non-equilibrium physics in determining the  $\alpha$ -transition.

### C. Signature of transition point through genuine multipartite entanglement

Upto now all the measures employed for detecting  $\alpha$ -transition do not capture the genuine multipartite features. Let us now explore the potential of genuine multipartite entanglement measure, namely generalized geometric measure (GGM) in the context of carrying signature of  $\alpha$ -transition. Mathematically, the GGM,  $\mathcal{G}$ , of a pure state  $|\psi\rangle$  is defined as

$$\mathcal{G}(|\psi\rangle) = 1 - \max_{A:B} \{\lambda_{A:B}^2 | A \cup B = \{1, 2, \dots, N\}, A \cap B = \emptyset\}, \quad (3)$$

where the maximization is over all possible bipartitions  $A$  and  $B$  of the whole system, and  $\lambda_{A:B}$  denotes the corresponding Schmidt coefficients. Although  $\mathcal{G}$  is hard to compute for a generic state with large number of sites due to the increasing number of partitions, an extensive numerical search indicates that if the system-size is large enough, i.e.,  $N \geq 9$  for  $d = 3$ , the maximum Schmidt coefficient that contributes in the GGM is solely from the bipartition  $A = \{1\}, B = \{2, 3, 4, \dots, N\}$  (see Appendix C).

First, we notice that  $\mathcal{G}(N, \alpha, d, t)$  for the dynamical state,  $|\psi(t)\rangle$  achieves its maximum value  $\mathcal{G}_{\max} = 1 - \frac{1}{d}$  at  $t = \frac{2\pi}{d}$  for all fall-off rates  $\alpha$  (see Fig. 5). Secondly, for high values of  $\alpha$ , i.e., when the system approaches to the nearest-neighbor model,  $\mathcal{G}$  vanishes at  $t = 2\pi$  while  $\mathcal{G}$  vanishes for  $t = 2n\pi \forall n \in \mathbb{Z}$  periodically. Depending on the strength of the fall-off rate  $\alpha$ , GGM becomes non-vanishing at  $t = 2\pi$ , irrespective of the dimension in the individual site. Therefore,

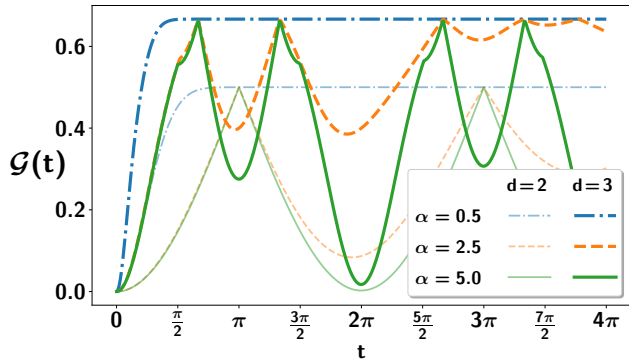


FIG. 5. (Color online.) GGM,  $\mathcal{G}$  (vertical axis) against time  $t$  (horizontal axis) of the WGS. Here  $N = 1000$  (dark shade for  $d = 3$  and light shade for  $d = 2$ ). Solid, dashed and dashed-dotted lines represent  $\alpha = 5.0, 2.5$  and  $0.5$  respectively. Note that  $\mathcal{G}$  reaches first maximum value  $0.5(d = 2)$  and  $0.6667(d = 3)$  at  $t = \frac{2\pi}{d}$  while  $\mathcal{G}$  vanishes for high  $\alpha$  with  $t = 2\pi$  and remains non-vanishing for low values of  $\alpha$ , thereby carrying signature  $\alpha$ . Note that Both the axes are dimensionless.

the deviation of  $\mathcal{G}$  from vanishing  $\mathcal{G}$  at  $t = 2\pi$  is competent to signal  $\alpha$  dependence in the system. Specifically, we compute at  $t = 2\pi$

$$\bar{\mathcal{G}}_\alpha = \frac{d\mathcal{G}(\alpha, d, 2\pi)}{d\alpha} \quad \text{and} \quad \bar{\mathcal{G}}_t = \left. \frac{d\mathcal{G}(\alpha, d, t)}{dt} \right|_{2\pi}, \quad (4)$$

and manifest that they both can be used to detect the NL to QL transition point (see Ref. [93] for spin-1/2). For each local spin dimension  $d$ ,  $\bar{\mathcal{G}}_\alpha$ , remains vanishing upto some low values of  $\alpha$ , the slope starts to acquire negative value as  $\alpha$  increases and after reaching a minimum, it shoots up to a positive value, exhibiting a discontinuous jump which matches the critical value  $\alpha_d^*$  predicted by  $\langle I \rangle_t$ . For  $\alpha > \alpha_d^*$ ,  $\bar{\mathcal{G}}_\alpha$  monotonically decreases with  $\alpha$  and remains negative for high  $\alpha$  (see in Fig. 6). More specifically the discontinuities for various  $d$  are obtained at  $\alpha_2^* = 1.000, \alpha_3^* = 1.585, \alpha_4^* = 2.000$  and  $\alpha_5^* = 2.322$ , upto third decimal place which are identical with the one obtained from the time averaged mutual information. This analysis again reveals that  $\alpha_d^*$  obtained from the non-analytic behavior of  $\mathcal{G}_\alpha$  are increasing with the increase of the dimension  $d$  of the individual site and it scales as  $\sim \log_2 d$  (as clearly depicted in the inset of Fig. 6).

#### IV. INDICATION OF TRANSITION TO LOCAL REGIME IN HIGHER DIMENSIONAL SYSTEMS

It is interesting to note that the  $\alpha$ -transition is different from the critical points corresponding to the quantum phase transition which is typically revealed from the vanishing energy gaps. Moreover, it was realized that quasi-local to local transition is again harder to detect from the features of quantum states in comparison with non-local to (quasi)local transition. Even in spin-1/2 systems, such transitions (QL to local) through the properties of the WGS is delicate to identify which is known from the other method.

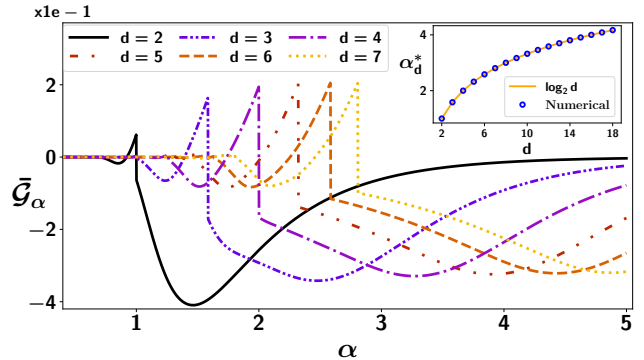


FIG. 6. (Color online.) Detection of  $\alpha$ -transition point through GGM. Trends of  $\bar{\mathcal{G}}_\alpha$  (ordinate) of the WGS at a fixed time  $t = 2\pi$  as a function of fall-off rate  $\alpha$  (abscissa) for different values of  $d = 2, 3, 4, 5, 6$  and  $7$ . The value of  $\alpha$  at which the discontinuity of  $\bar{\mathcal{G}}_\alpha$  is observed increases with the increase in the local spin quantum number, thereby predicting  $\alpha = \alpha_d^*$ . (Inset) By fitting the numerical values of  $\alpha_d^*$  with the dimension  $d$  (upto  $d = 18$ ), we find the dependence of  $\alpha$ -transition point on  $d$  as  $\alpha_d^* \sim \log_2 d$  which is in good agreement with the results obtained from  $\bar{A}_\alpha$  in Fig. 4. Both the axes are dimensionless.

Based on the pattern of GGM in the dynamical state, we define time averaged GGM,  $\langle \mathcal{G}(N, \alpha, d) \rangle_t = \frac{\int_0^{t_0} \mathcal{G}(N, \alpha, d, t) dt}{t_0}$ , where the initial state at  $t = 0$  evolve till  $t = t_0$  (see similar definition for MI in previous section).

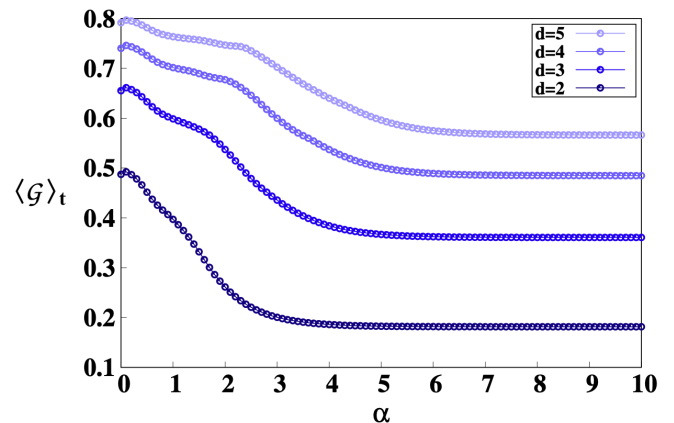


FIG. 7. (Color online.) The time-averaged value of GGM,  $\langle \mathcal{G} \rangle_t$  (vertical axis) vs  $\alpha$  (horizontal axis) for different values of  $d$  in the individual sites. The averaging in  $\langle \mathcal{G} \rangle_t$  is performed from  $t = 0$  to  $t = 3\pi$ . Here  $N = 10^3$ . Both the axes are dimensionless.

We observe that as the fall-off exponent  $\alpha$  decreases,  $\langle \mathcal{G}(N, \alpha, d) \rangle_T$  decreases with  $\alpha$  and saturates for a certain  $\alpha$  value (see Fig. 5). Examining the behavior of GGM during evolution, we choose  $t_0 = 3\pi$  and find that the saturated GGM value increases with the increase in the dimension of the local sites (e.g.  $\langle \mathcal{G} \rangle_{3\pi} = 0.18, 0.36, 0.48, 0.56$  for  $d = 2, 3, 4, 5$  respectively). Surprisingly, for the qubit system we observe that

the time averaged GGM starts saturating after  $\alpha \gtrsim 2 \equiv \alpha_2^{**}$ , which differentiates local region from QL one.

Up to our knowledge, there is no clear evidence of this kind of transition point for lattice with higher spin quantum number. The trends of  $\langle \mathcal{G} \rangle_t$  strongly suggest the existence of  $\alpha_d^{**}$  as a second transition point for higher dimensions which also depends on the dimension of the individual site as established for  $\alpha_d^*$  (see Fig. 7). Specifically, we estimate  $\alpha_d > \alpha_d^S$ , (with  $\alpha_d^S$  being the value where  $\langle \mathcal{G} \rangle_t$  saturates) which belongs to the local regime. To obtain more precise estimation of  $\alpha_d^{**}$ , we explore the dependence of  $\langle \mathcal{G} \rangle_t$  on total number of qudits  $N$ , in the lattice. In particular, we compute

$$\Delta \langle \mathcal{G}(\alpha, d) \rangle_{N_{sat}} \equiv \min_N |\langle \mathcal{G}(N+1, \alpha, d) \rangle_t - \langle \mathcal{G}(N, \alpha, d) \rangle_t| < \epsilon, \quad (5)$$

which leads to a quantity, called  $N_{sat}$ , above which  $\langle \mathcal{G} \rangle_t$  remains unaltered for a given error window  $\epsilon < 10^{-v}$ .

For the lattice with spin-1 particles, by fixing  $\epsilon = 10^{-v}$  with  $v = 2, 3, 4, 5$ ,  $N_{sat}$  remains same for  $\alpha \gtrsim 3.5$  for any value of  $\epsilon$  as depicted in Fig. 8 while analogous analysis for spin-1/2 reveals  $\alpha_2^{**} \approx 2$ .

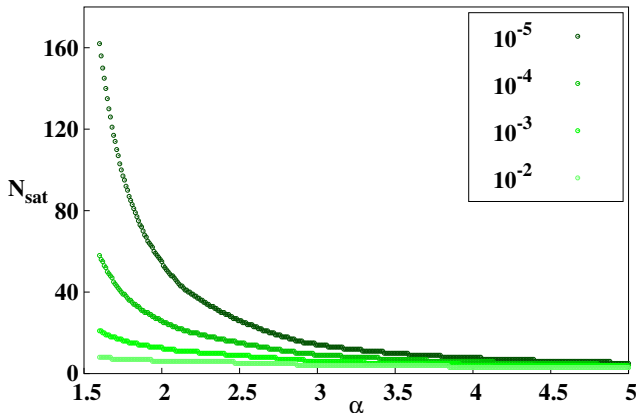


FIG. 8. (Color online.) Saturation value of the number of qudits,  $N_{sat}$  (ordinate) against  $\alpha$  (abscissa) for different values of error,  $\epsilon$  (mentioned in legends). Irrespective of  $\epsilon$ ,  $N_{sat}$  turns out to be same and finite for  $\alpha \gtrsim 3.5$ , signalling QL to local transition. Both the axes are dimensionless.

Therefore, the investigation of both  $\langle \mathcal{G} \rangle_t$  and  $N_{sat}$  can strongly indicate another transition,  $\alpha_d^{**}$  of the transverse spin- $s$  Ising model and its dependence on the spin quantum number. However, unlike  $\alpha_d^*$ , the precise estimation of  $\alpha_d^{**}$  cannot be predicted from the entangled dynamics of the WGS.

## V. CONCLUSION

The elegance of a one-way quantum computer is the notion of creating a highly entangled state in a physically realizable system on which a universal set of quantum gates can be implemented using local measurements. Although the original proposal is for lattice containing spin-1/2 particles,

it was extended to qudit cluster states, generated from higher dimensional Ising-type (NN) interactions as the foundational framework for execution of higher dimensional measurement-based quantum computation (MBQC). It was also realized that while implementing MBQC in trapped ions or other physical systems, it is natural to consider evolving Hamiltonian with variable-range interaction which was recently considered for spin-1/2 system from the perspective of entanglement profile. This work concentrates on revealing features of the evolving Hamiltonian based on the trends of the information-theoretic quantities when the individual site is occupied by a  $d$ -dimensional quantum state, a qudit. By choosing spin- $s$  variable-range Ising Hamiltonian for evolution with the initial state being chosen to be the maximally coherent state in that dimension at individual lattice site, one can create a multi-qudit weighted graph state, which depends on the time, dimension and, more importantly, the range of interaction quantified by the fall-off rate parameter,  $\alpha$ . By inspecting the block entanglement entropy at a fixed time with the variation of the length of the block, we established that there exists at least one transition in  $\alpha$  from nonlocal to local regimes which can again be confirmed from the dynamical behavior of mutual information between two arbitrary qudits situated in two distant lattice sites. However, the precise  $\alpha$ -transition point and its dependence on spin quantum number can only be predicted by the scaling law of the time-averaged mutual information and the derivative of genuine multipartite entanglement measure with respect to  $\alpha$  for a fixed time at which the entanglement vanishes for the nearest-neighbor model. Both the quantities suggest that the variation of the first  $\alpha$ -transition scales logarithmically with the dimension of a single site which coincides in the case of the spin-1/2 system that is known in literature.

The time-averaged multipartite entanglement as well as its dependence on system-size possibly signal the existence of another  $\alpha$ -transition, namely quasi-local to local one as it was known for the spin-1/2 system. However, our analysis based on the WGS cannot accurately predict this  $\alpha$ -transition point. We believe that our work not only establishes the power of quantum information-theoretic quantities in determining non-equilibrium physics but also sheds light on the prediction of different kinds of  $\alpha$ -transition in arbitrary spin- $s$  systems which is typically hard to address by both numerical and analytical procedures.

## ACKNOWLEDGMENTS

We acknowledge the support from Interdisciplinary Cyber Physical Systems (ICPS) program of the Department of Science and Technology (DST), India, Grant No.: DST/ICPS/QuST/Theme- 1/2019/23. We acknowledge the use of QIClib – a modern C++ library for general purpose quantum information processing and quantum computing (<https://titaschanda.github.io/QIClib>) and cluster computing facility at Harish-Chandra Research Institute.

## Appendix A: Reduced density matrix of weighted graph states

Let us divide the whole  $N$ -site lattice into two subsystems,  $A$  and  $\bar{A}$  where  $\bar{A}$  is the complement of  $A$ , i.e.,  $A \cup \bar{A}$  constitute the whole system. We can write the reduced state,  $\rho_A$ , for the commuting unitary  $U_{ij}$ , defined in Sec. II as

$$\rho_A = \prod_{i,j \in A} U_{ij} \rho'_A U_{ij}^\dagger. \quad (\text{A1})$$

Note that the unitaries acting only on the qudits in  $\bar{A}$  does not effect the subsystem  $\rho_A$ . The unitaries acting on each site from  $A$  and  $\bar{A}$  leads to a state

$$|\psi'\rangle = \prod_{k \in A, l \in \bar{A}} U_{kl} |+\rangle^{\otimes N}, \quad (\text{A2})$$

from which we get the reduced state as  $\rho'_A = \text{Tr}_{\bar{A}} |\psi'\rangle \langle \psi'|$ . In the PEPS picture, every qudit of a  $N$ -qudit state is replaced by  $N-1$  virtual qudits. Here, the virtual qudits of the subsystem  $\bar{A}$  is connected with the virtual qudits of  $A$  by the unitaries  $U_{kl}$ . Acting projectors  $P_m$  of the form

$$P_m = \sum_{k=0}^{d-1} |k_m\rangle \langle \mathbf{k}_m|, \quad (\text{A3})$$

with  $|\mathbf{k}_m\rangle = |k_1 k_2 \dots k_{m-1} k_{m+1} \dots k_N\rangle$  on  $\bar{A}$  subsystem, we obtain the state where all the qudits of  $\bar{A}$  is entangled with the virtual qudits of  $A$ . For each of the virtual entangled state, the reduced density operator,  $\rho'_A(l)$  of  $A$  corresponding to each  $l \in \bar{A}$  can be obtained by tracing out the  $l$ th party. So the reduce density can be written as

$$\rho'_A(l) = \frac{1}{d} \sum_{r=0}^{d-1} |\phi_l^r\rangle \langle \phi_l^r|; |\phi_l^r\rangle = \bigotimes_{k \in A} \sum_{\mu=0}^{d-1} \frac{e^{ir\mu g_{kl} t}}{\sqrt{d}} |\mu\rangle. (\text{A4})$$

Now,  $\rho'_A$  can be obtained by performing Hadamard product of all  $\rho'_A(l) \forall l \in \bar{A}$  when we take projections in  $A$ . In this fashion, all the reduced density matrices of the WGS can be obtained. Note, however, that to calculate any quantum information theoretic quantities, we shall require to diagonalize these matrices which are, in general, hard to obtain.

## Appendix B: Oscillation in mutual information for multiqubit WGS

In the case of spin-1/2 system, the mutual information with respect to time behaves similarly as shown in the case of spin-1 system for different  $\alpha$  values (see Fig. 2 for multiqutrit systems and Fig. 9 for multiqubit WGS). The maximum of MI is again obtained for the nearest-neighbor sites. Instead of a single oscillation for  $\alpha < 1$ , more oscillations in MI with time appear as  $\alpha$  is increased.

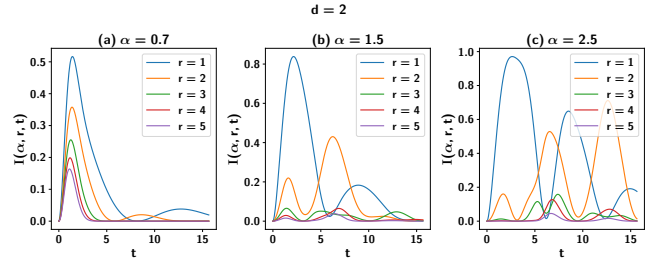


FIG. 9. (Color online.) Mutual information,  $I(\alpha, r, t)$  (vertical axis) against time  $t$  (horizontal axis) for the various fall-off rates  $\alpha$  (a)-(c) for spin-1/2 Ising Hamiltonian with open boundary condition used for evolution. Here  $N = 10^3$ . Different lines represent different values of  $r$ . Both the axes are dimensionless.

## Appendix C: Calculation of GGM of multiqutrit WGS and its behavior

In general, for large system sizes, multipartite entanglement is hard to compute, as the multipartite entanglement should be non-vanishing if and only if the state is not separable across any bipartition. We choose generalized geometric measure as the quantifier of genuine multipartite entanglement. It was recently shown that for the multiqubit WGS, GGM is obtained from the single-site reduced density matrix lying at the edge of the chain, i.e., the maximum required for GGM achieved from  $\rho_1$  [93]. We show that the same analysis follows for the multiqutrit WGS. First of all, for multiqutrit WGS, we see that the GGM is highly sensitive to the system-size, especially near  $t = 2\pi$ , as illustrated in Fig. 10. Such  $N$ -dependence of GGM around  $t = 2\pi$  is true for all values of  $\alpha$ . It also provides an evidence that  $t = 2\pi$  in the context of multipartite entanglement is special.

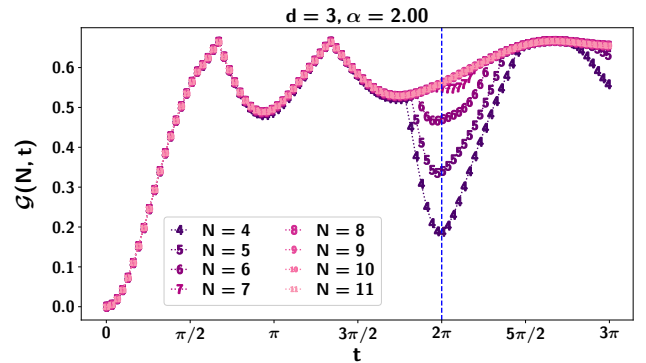


FIG. 10. (Color online.) GGM (vertical axis) as a function of time (horizontal axis) for multiqutrit WGS. The exact value of  $\mathcal{G}(N, t)$  is computed for different system-sizes at fixed  $\alpha = 2.0$ . For most of the times till  $t = 2\pi$ , GGM is almost insensitive to the system-size, although GGM clearly depends on  $N$  around  $t = 2\pi$ . However, the dynamical GGM-profile saturates for large system sizes even at  $t = 2\pi$ . Both the axes are dimensionless.

Let us now argue that for large  $N$ , if we compute GGM by considering the maximum eigenvalue of  $\rho_1$ , the error is negli-

gible. To compute the average error, we consider  $\mathcal{E}(N, \alpha) = \langle |\mathcal{G}(N, \alpha, t) - \mathcal{G}_1(N, \alpha, t)| \rangle_t$ , where the average  $\mathcal{G}(N, \alpha, t)$  and  $\mathcal{G}_1(N, \alpha, t)$  denote the actual GGM and the GGM computed with the assumption that  $\rho_1$  gives the maximum eigenvalue respectively and the average is taken from  $t = 0$  to  $t_0 = 3\pi$ .

The error  $\mathcal{E}(N, \alpha)$ , decreases exponentially with the system-size  $N$ , as shown in Fig. 11.  $\mathcal{E}(N, \alpha) < 10^{-3}$  upto  $N = 11$ , and is steadily decreasing (exponentially with  $N$ ) for all fall-off rates  $\alpha$ . This suggests that like in the qubit ( $d = 2$ ) case, GGM for large system-size  $N$  can be computed efficiently from the single side reduced density matrix of the edge for any  $d$ . In case of  $d = 4$ , this extensive numerical verification is hard and computations are restricted upto  $N = 7$ . This analysis also mimics the similar behavior and, therefore, this analysis can be generalised for higher value of  $d$  as well. From this investigation, we safely call  $\mathcal{G}_1(N, \alpha, t)$  as  $\mathcal{G}(N, \alpha, t)$ .

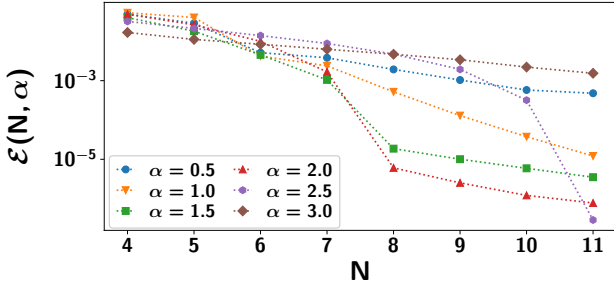


FIG. 11. (Color online.) Error (vertical axis) between the actual GGM  $\mathcal{G}$  and the estimated GGM  $\mathcal{G}_1$  with system-size  $N$ . The error decreases exponentially for large  $N$ . The vertical axis is in logarithmic scale and both the axes are dimensionless.

As we have shown in Fig. 6, let us demonstrate here that the time derivative of GGM can also determine the NL to QL transition point in the fall-off rate  $\alpha$ . The time derivative of GGM at  $t = 2\pi$ , denoted as  $\bar{\mathcal{G}}_t$ , shows non-analyticity at same  $\alpha$  values as those for  $\bar{\mathcal{G}}_\alpha$  Sec. III C (comparing Figs. 6 and Fig. 12). Therefore, both  $\bar{\mathcal{G}}_\alpha$  and  $\bar{\mathcal{G}}_t$  at  $t = 2\pi$  can detect the NL to QL transition point in  $\alpha$ .

#### Appendix D: Reducing number of qudits in WGS by local measurements

We report here that the effect of local measurements on a single qudit of this all-to-all connected WGS is equivalent to the known results for multiqubit system [93]. Measurement along a specific direction on WGS produce a local unitary

equivalent WGS with a lesser numbers of qudits than the input. It can serve as a resource for  $d$ -level quantum computation.

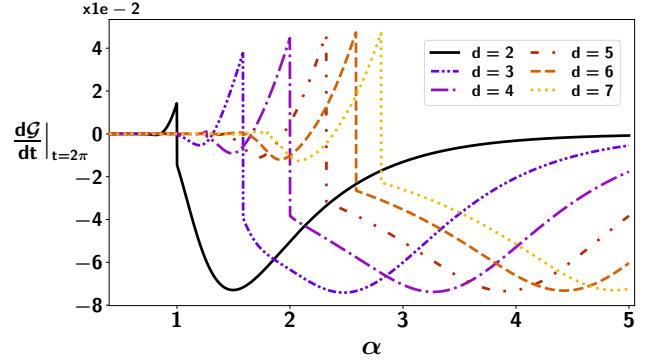


FIG. 12. (Color online.) Detection of  $\alpha$ -transition point through time derivative of GGM. Variation of  $\bar{\mathcal{G}}_t$  (ordinate) of the multiqubit WGS at time  $t = 2\pi$  against the fall-off rate  $\alpha$  (abscissa) for local spin dimension  $d = 2, 3, 4, 5, 6$  and  $7$ . The values of  $\alpha$  at which the discontinuity of  $\bar{\mathcal{G}}_t$  occur, are same as given by  $\bar{\mathcal{G}}_\alpha$  (see Fig. 6). Both the axes are dimensionless.

By considering  $N$ -qudit WGS,

$$\begin{aligned} & |G(t)\rangle_{N\{1,2,\dots,k,\dots,N\}} \\ &= \frac{1}{d^{N/2}} \sum_{\eta=0}^{d^{N-1}-1} \left( \prod_{\substack{i,j=1 \\ i < j}}^N \exp(ia_i a_j \phi_{ij}) |\eta\rangle \right), \quad (\text{D1}) \end{aligned}$$

We perform measurement in generalized  $Z$ -basis  $\{|m\rangle\}_0^{d-1}$ , i.e., in the eigenstate of  $Z_d = \sum_{k=0}^{d-1} q_d^k |k\rangle \langle k|$ , where  $q_d = \exp\left[\frac{i2\pi}{d}\right]$ . The output state after measurement on  $k$ th qudit is local unitarily equivalent to

$$\begin{aligned} & |G(t)\rangle_{(N-1)\{1,2,\dots,k-1,k+1,\dots,N\}} \\ &= \frac{1}{d^{(N-1)/2}} \sum_{\zeta=0}^{d^{N-1}-1} \left( \prod_{\substack{i,j=1 \\ i < j \\ i,j \neq k}}^N \exp(ia_i a_j \phi_{ij}) |\eta\rangle \right), \end{aligned}$$

where  $|\zeta\rangle \equiv |a_1 a_2 \dots a_{k-1} a_{k+1} \dots a_N\rangle$  with  $a_i = 0, 1, \dots, d-1$  and  $\zeta$  being decimal equivalent of computational basis  $\{|a_1 a_2 \dots a_N\rangle\}$  (addition modulo  $d$ ). Similarly, after performing such measurements on  $m$  number of qudits, we obtain a state, which is local unitarily equivalent to  $|G(t)\rangle$  of  $N - m$  qudits.

[1] M. A. Nielsen and I. L. Chuang, *Quantum Computation and Quantum Information* (Cambridge University Press, 2009).  
[2] P. Horodecki, *Physics Letters A* **232**, 333 (1997).

[3] M. Horodecki, P. Horodecki, and R. Horodecki, *Phys. Rev. Lett.* **80**, 5239 (1998).  
[4] T. Kraft, C. Ritz, N. Brunner, M. Huber, and O. Gühne, *Phys.*

- Rev. Lett. **120**, 060502 (2018).
- [5] D. Collins, N. Gisin, N. Linden, S. Massar, and S. Popescu, *Phys. Rev. Lett.* **88**, 040404 (2002).
- [6] W. Son, J. Lee, and M. S. Kim, *Phys. Rev. Lett.* **96**, 060406 (2006).
- [7] A. C. Dada, J. Leach, G. S. Buller, M. J. Padgett, and E. Andersson, *Nature Physics* **7**, 677 (2011).
- [8] H. Bechmann-Pasquinucci and W. Tittel, *Phys. Rev. A* **61**, 062308 (2000).
- [9] N. J. Cerf, M. Bourennane, A. Karlsson, and N. Gisin, *Phys. Rev. Lett.* **88**, 127902 (2002).
- [10] G. M. Nikolopoulos, K. S. Ranade, and G. Alber, *Phys. Rev. A* **73**, 032325 (2006).
- [11] L. Sheridan and V. Scarani, *Phys. Rev. A* **82**, 030301 (2010).
- [12] T. Sasaki, Y. Yamamoto, and M. Koashi, *Nature* **509**, 475 (2014).
- [13] F. Bouchard, K. Heshami, D. England, R. Fickler, R. W. Boyd, B.-G. Englert, L. L. Sanchez-Soto, and E. Karimi, *Quantum* **2**, 111 (2018).
- [14] D. Cozzolino, D. Bacco, B. Da Lio, K. Ingerslev, Y. Ding, K. Dalgaard, P. Kristensen, M. Galili, K. Rottwitt, S. Ramachandran, and L. K. Oxenløwe, *Phys. Rev. Appl.* **11**, 064058 (2019).
- [15] M. Arajo, M. Huber, M. Navascus, M. Pivoluska, and A. Tavakoli, *Quantum* **7**, 1019 (2023).
- [16] L. Bulla, M. Pivoluska, K. Hjorth, O. Kohout, J. Lang, S. Ecker, S. P. Neumann, J. Bittermann, R. Kindler, M. Huber, M. Bohmann, and R. Ursin, *Phys. Rev. X* **13**, 021001 (2023).
- [17] M. Neeley, M. Ansmann, R. C. Bialczak, M. Hofheinz, E. Lucero, A. D. O’Connell, D. Sank, H. Wang, J. Wenner, A. N. Cleland, M. R. Geller, and J. M. Martinis, *Science* **325**, 722 (2009).
- [18] R. Kaltenbaek, J. Lavoie, B. Zeng, S. D. Bartlett, and K. J. Resch, *Nature Physics* **6**, 850 (2010).
- [19] E. Nagali, D. Giovannini, L. Marrucci, S. Slussarenko, E. Santamato, and F. Sciarrino, *Phys. Rev. Lett.* **105**, 073602 (2010).
- [20] F. Bouchard, R. Fickler, R. W. Boyd, and E. Karimi, *Science Advances* **3** (2017), 10.1126/sciadv.1601915.
- [21] M. Marciniak, A. Rutkowski, Z. Yin, M. Horodecki, and R. Horodecki, *Phys. Rev. Lett.* **115**, 170401 (2015).
- [22] V. Srivastav, N. H. Valencia, W. McCutcheon, S. Leedumrongwathanakun, S. Designolle, R. Uola, N. Brunner, and M. Malik, *Phys. Rev. X* **12**, 041023 (2022).
- [23] A. Patra, R. Gupta, T. Das, and A. S. De, “Dimensional advantage in secure information trading via the noisy dense coding protocol,” (2023), [arXiv:2310.20688 \[quant-ph\]](https://arxiv.org/abs/2310.20688).
- [24] L. A. Correa, *Phys. Rev. E* **89**, 042128 (2014).
- [25] J. Wang, Y. Lai, Z. Ye, J. He, Y. Ma, and Q. Liao, *Phys. Rev. E* **91**, 050102 (2015).
- [26] A. C. Santos, B. i. e. i. f. m. c. Çakmak, S. Campbell, and N. T. Zinner, *Phys. Rev. E* **100**, 032107 (2019).
- [27] F.-Q. Dou, Y.-J. Wang, and J.-A. Sun, *EPL (Europhysics Letters)* **131**, 43001 (2020).
- [28] A. Usui, W. Niedenzu, and M. Huber, *Phys. Rev. A* **104**, 042224 (2021).
- [29] S. Ghosh and A. Sen(De), *Phys. Rev. A* **105**, 022628 (2022).
- [30] T. K. Konar, S. Ghosh, A. K. Pal, and A. Sen(De), *Phys. Rev. A* **107**, 032602 (2023).
- [31] C. K. Lai, *Journal of Mathematical Physics* **15**, 1675 (1974).
- [32] B. Sutherland, *Phys. Rev. B* **12**, 3795 (1975).
- [33] L. Takhtajan, *Physics Letters A* **87**, 479 (1982).
- [34] H. Babujian, *Physics Letters A* **90**, 479 (1982).
- [35] I. Affleck, T. Kennedy, E. H. Lieb, and H. Tasaki, *Phys. Rev. Lett.* **59**, 799 (1987).
- [36] G. Fáth and J. Sólyom, *Phys. Rev. B* **44**, 11836 (1991).
- [37] G. Fáth and J. Sólyom, *Phys. Rev. B* **47**, 872 (1993).
- [38] K. Buchta, G. Fáth, O. Legeza, and J. Sólyom, *Phys. Rev. B* **72**, 054433 (2005).
- [39] R. Mao, Y.-W. Dai, S. Y. Cho, and H.-Q. Zhou, *Phys. Rev. B* **103**, 014446 (2021).
- [40] M. Blume, V. J. Emery, and R. B. Griffiths, *Phys. Rev. A* **4**, 1071 (1971).
- [41] J. Sivardièrre and M. Blume, *Phys. Rev. B* **5**, 1126 (1972).
- [42] A. Kolezhuk, R. Roth, and U. Schollwöck, *Phys. Rev. Lett.* **77**, 5142 (1996).
- [43] D. L. Zhou, B. Zeng, Z. Xu, and C. P. Sun, *Phys. Rev. A* **68**, 062303 (2003).
- [44] E. Hostens, J. Dehaene, and B. De Moor, *Phys. Rev. A* **71**, 042315 (2005).
- [45] W. Hall, [arXiv preprint quant-ph/0512130](https://arxiv.org/abs/quant-ph/0512130) (2005).
- [46] J. Joo, P. L. Knight, J. L. O’Brien, and T. Rudolph, *Phys. Rev. A* **76**, 052326 (2007).
- [47] D. H. Zhang, H. Fan, and D. L. Zhou, *Phys. Rev. A* **79**, 042318 (2009).
- [48] D.-S. Wang, D. T. Stephen, and R. Raussendorf, *Phys. Rev. A* **95**, 032312 (2017).
- [49] Y. Wang, Z. Hu, B. C. Sanders, and S. Kais, *Frontiers in Physics* **8** (2020), 10.3389/fphy.2020.589504.
- [50] R. I. Booth, A. Kissinger, D. Markham, C. Meignant, and S. Perdrix, *Journal of Physics A: Mathematical and Theoretical* **56**, 115303 (2023).
- [51] F. K. Marquversen and N. T. Zinner, (2023), 10.1088/2058-9565/ace2e6.
- [52] *npj Quantum Information* **5**, 59 (2019).
- [53] *New Journal of Physics* **22**, 013027 (2020).
- [54] P. J. Low, B. M. White, A. A. Cox, M. L. Day, and C. Senko, *Physical Review Research* **2**, 033128 (2020).
- [55] P. Hrmo, B. Wilhelm, L. Gerster, M. W. van Mourik, M. Huber, R. Blatt, P. Schindler, T. Monz, and M. Ringbauer, *Nature Communications* **14** (2023), 10.1038/s41467-023-37375-2.
- [56] H. F. Chau, *Phys. Rev. A* **56**, R1 (1997).
- [57] S. L. Braunstein, *Phys. Rev. Lett.* **80**, 4084 (1998).
- [58] D. Hu, W. Tang, M. Zhao, Q. Chen, S. Yu, and C. H. Oh, *Phys. Rev. A* **78**, 012306 (2008).
- [59] M. Grassl, L. Kong, Z. Wei, Z.-Q. Yin, and B. Zeng, *IEEE Transactions on Information Theory* **64**, 4674 (2018).
- [60] L. G. Gunderman, *Phys. Rev. A* **101**, 052343 (2020).
- [61] F. Schmidt and P. van Loock, *Phys. Rev. A* **105**, 042427 (2022).
- [62] L. G. Gunderman, *Phys. Rev. A* **105**, 042424 (2022).
- [63] S. Sachdev, *Quantum Phase Transitions*, 2nd ed. (Cambridge University Press, 2011).
- [64] A. Campa, T. Dauxois, D. Fanelli, and S. Ruffo, *Physics of Long-Range Interacting Systems* (Oxford University Press Oxford, 2014).
- [65] N. Maskara, A. Deshpande, A. Ehrenberg, M. C. Tran, B. Fefferman, and A. V. Gorshkov, *Phys. Rev. Lett.* **129**, 150604 (2022).
- [66] N. Defenu, T. Donner, T. Macri, G. Pagano, S. Ruffo, and A. Trombettoni, *Rev. Mod. Phys.* **95**, 035002 (2023).
- [67] H. HAFFNER, C. ROOS, and R. BLATT, *Physics Reports* **469**, 155 (2008).
- [68] A. Friedenauer, H. Schmitz, J. T. Glueckert, D. Porras, and T. Schaetz, *Nature Physics* **4**, 757.
- [69] K. Kim, M.-S. Chang, R. Islam, S. Korenblit, L.-M. Duan, and C. Monroe, *Phys. Rev. Lett.* **103**, 120502 (2009).
- [70] A. Khromova, C. Piltz, B. Scharfenberger, T. F. Gloger, M. Jo-

- hanning, A. F. Varón, and C. Wunderlich, *Phys. Rev. Lett.* **108**, 220502 (2012).
- [71] R. Islam, E. Edwards, K. Kim, S. Korenblit, C. Noh, H. Carmichael, G.-D. Lin, L.-M. Duan, C.-C. J. Wang, J. Freericks, and C. Monroe, *Nature Communications* **2**, 377 (2011).
- [72] J. W. Britton, B. C. Sawyer, A. C. Keith, C.-C. J. Wang, J. K. Freericks, H. Uys, M. J. Biercuk, and J. J. Bollinger, *Nature* **484**, 489 (2012).
- [73] D. Porras and J. I. Cirac, *Phys. Rev. Lett.* **92**, 207901 (2004).
- [74] J. yoon Choi, S. Hild, J. Zeiher, P. Schau, A. Rubio-Abadal, T. Yefsah, V. Khemani, D. A. Huse, I. Bloch, and C. Gross, *Science* **352**, 1547 (2016).
- [75] M. Rispoli, A. Lukin, R. Schittko, S. Kim, M. E. Tai, J. Lonard, and M. Greiner, *Nature* **573**, 385 (2019).
- [76] O. Mandel, M. Greiner, A. Widera, T. Rom, T. W. Hnsch, and I. Bloch, *Nature* **425**, 937 (2003).
- [77] M. Cramer, A. Bernard, N. Fabbri, L. Fallani, C. Fort, S. Rosi, F. Caruso, M. Inguscio, and M. Plenio, *Nature Communications* **4**, 2161 (2013).
- [78] R. Landig, L. Hruby, N. Dogra, M. Landini, R. Mottl, T. Donner, and T. Esslinger, *Nature* **532**, 476 (2016).
- [79] C. Gross and I. Bloch, *Science* **357**, 995 (2017).
- [80] A. Camacho-Guardian, R. Paredes, and S. F. Caballero-Benítez, *Phys. Rev. A* **96**, 051602 (2017).
- [81] S. Rasmussen, K. Christensen, S. Pedersen, L. Kristensen, T. Bækkegaard, N. Loft, and N. Zinner, *PRX Quantum* **2**, 040204 (2021).
- [82] C. Ying, B. Cheng, Y. Zhao, H.-L. Huang, Y.-N. Zhang, M. Gong, Y. Wu, S. Wang, F. Liang, J. Lin, Y. Xu, H. Deng, H. Rong, C.-Z. Peng, M.-H. Yung, X. Zhu, and J.-W. Pan, *Phys. Rev. Lett.* **130**, 110601 (2023).
- [83] J. Zhang, G. Pagano, P. W. Hess, A. Kyprianidis, P. Becker, H. Kaplan, A. V. Gorshkov, Z.-X. Gong, and C. Monroe, *Nature* **551**, 601 (2017).
- [84] N. Defenu, G. Morigi, L. Dell’Anna, and T. Enss, *Phys. Rev. B* **100**, 184306 (2019).
- [85] J. C. Halimeh, M. Van Damme, V. Zauner-Stauber, and L. Vanderstraeten, *Phys. Rev. Res.* **2**, 033111 (2020).
- [86] L. G. C. Lakkaraju, S. Ghosh, D. Sadhukhan, and A. S. De, “Framework of dynamical transitions from long-range to short-range quantum systems,” (2023), [arXiv:2305.02945 \[quant-ph\]](https://arxiv.org/abs/2305.02945).
- [87] N. Defenu, *Proceedings of the National Academy of Sciences* **118** (2021), [10.1073/pnas.2101785118](https://doi.org/10.1073/pnas.2101785118).
- [88] G. Giachetti and N. Defenu, *Scientific Reports* **13**, 12388 (2023).
- [89] C.-F. Chen and A. Lucas, *Phys. Rev. Lett.* **123**, 250605 (2019).
- [90] M. C. Tran, C.-F. Chen, A. Ehrenberg, A. Y. Guo, A. Deshpande, Y. Hong, Z.-X. Gong, A. V. Gorshkov, and A. Lucas, *Phys. Rev. X* **10**, 031009 (2020).
- [91] T. Kuwahara and K. Saito, *Phys. Rev. X* **10**, 031010 (2020).
- [92] T. Anuradha, A. Patra, R. Gupta, A. Rai, and A. S. De, “Production of genuine multimode entanglement in circular waveguides with long-range interactions,” (2023), [arXiv:2303.15137 \[quant-ph\]](https://arxiv.org/abs/2303.15137).
- [93] D. Ghosh, K. D. Agarwal, P. Halder, and A. S. De, “Entanglement of weighted graphs uncovers transitions in variable-range interacting models,” (2023), [arXiv:2307.11739 \[quant-ph\]](https://arxiv.org/abs/2307.11739).
- [94] A. Solfanelli, G. Giachetti, M. Campisi, S. Ruffo, and N. Defenu, *New Journal of Physics* **25**, 033030 (2023).
- [95] R. Yousefjani, X. H., and A. Bayat, *Chinese Physics B* **32**, 100313 (2023).
- [96] Monika, L. G. C. Lakkaraju, S. Ghosh, and A. S. De, “Better sensing with variable-range interactions,” (2023), [arXiv:2307.06901 \[quant-ph\]](https://arxiv.org/abs/2307.06901).
- [97] Z. Eldredge, Z.-X. Gong, J. T. Young, A. H. Moosavian, M. Foss-Feig, and A. V. Gorshkov, *Phys. Rev. Lett.* **119**, 170503 (2017).
- [98] M. C. Tran, A. Y. Guo, A. Deshpande, A. Lucas, and A. V. Gorshkov, *Phys. Rev. X* **11**, 031016 (2021).
- [99] D. Lewis, A. Benhemou, N. Feinstein, L. Banchi, and S. Bose, *Phys. Rev. Lett.* **126**, 240502 (2021).
- [100] D. Lewis, L. Banchi, Y. H. Teoh, R. Islam, and S. Bose, *Quantum Science and Technology* **8**, 035025 (2023).
- [101] T. Koffel, M. Lewenstein, and L. Tagliacozzo, *Phys. Rev. Lett.* **109**, 267203 (2012).
- [102] D. Vodola, L. Lepori, E. Ercolessi, A. V. Gorshkov, and G. Pupillo, *Phys. Rev. Lett.* **113**, 156402 (2014).
- [103] D. Vodola, L. Lepori, E. Ercolessi, and G. Pupillo, *New Journal of Physics* **18**, 015001 (2015).
- [104] N. Defenu, A. Codello, S. Ruffo, and A. Trombettoni, *Journal of Physics A: Mathematical and Theoretical* **53**, 143001 (2020).
- [105] J. Romn-Roche, V. Herriz-Lpez, and D. Zueco, “Exact solution for quantum strong long-range models via a generalized hubbard-stratonovich transformation,” (2023), [arXiv:2305.10482 \[quant-ph\]](https://arxiv.org/abs/2305.10482).
- [106] M. P. Kaicher, D. Vodola, and S. B. Jäger, *Phys. Rev. B* **107**, 165144 (2023).
- [107] L. Hartmann, J. Calsamiglia, W. Dr, and H. J. Briegel, *Journal of Physics B: Atomic, Molecular and Optical Physics* **40**, S1 (2007).
- [108] C. G. Brell, *New Journal of Physics* **17**, 023029 (2015).
- [109] Z.-X. Gong, M. Foss-Feig, F. G. S. L. Brandão, and A. V. Gorshkov, *Phys. Rev. Lett.* **119**, 050501 (2017).
- [110] W. Dür, L. Hartmann, M. Hein, M. Lewenstein, and H.-J. Briegel, *Phys. Rev. Lett.* **94**, 097203 (2005).
- [111] D. Vodola, L. Lepori, E. Ercolessi, and G. Pupillo, *New Journal of Physics* **18**, 015001 (2015).
- [112] J. Schachenmayer, B. P. Lanyon, C. F. Roos, and A. J. Daley, *Phys. Rev. X* **3**, 031015 (2013).
- [113] The exact calculation of  $S_L$  for different  $L$  values are performed numerically in which the maximum is restricted to efficient diagonalization of matrices possible numerically.